Plasmonic nano-bowls for monitoring intra-membrane changes in liposomes, and DNA-based nanocarriers in suspension

SATHI DAS,[1] **JEAN-CLAUDE TINGUELY,**[2] **SYBIL AKUA OKYEREWA OBUOBI,**[3] **NATAŠA ŠKALKO-BASNET,**[3] **KANCHAN SAXENA,**[4] **BALPREET SINGH AHLUWALIA,**[3,5] (ID) **AND DALIP SINGH MEHTA**[1,6]

[1]*Bio-photonics and Green Photonics Laboratory, Indian Institute of Technology Delhi, Hauz-Khas, New Delhi 110016, India*
[2] *Department of Physics and Technology, UiT The Arctic University of Norway, Tromsø 9037, Norway*
[3]*Drug Transport and Delivery Research Group, Department of Pharmacy, UIT The Arctic University of Norway, Tromsø, Norway*
[4]*Amity Institute of Renewable and Alternative Energy, Amity University Uttar Pradesh, Sector 125 Noida, U.P., India*
[5]*balpreet.singh.ahluwalia@uit.no*
[6]*mehtads@physics.iitd.ac.in*

Abstract: Programmable nanoscale carriers, such as liposomes and DNA, are readily being explored for personalized medicine or disease prediction and diagnostics. The characterization of these nanocarriers is limited and challenging due to their complex chemical composition. Here, we demonstrate the utilization of surface-enhanced Raman spectroscopy (SERS), which provides a unique molecular fingerprint of the analytes while reducing the detection limit. In this paper, we utilize a silver coated nano-bowl shaped polydimethylsiloxane (PDMS) SERS substrate. The utilization of nano-bowl surface topology enabled the passive trapping of particles by reducing mobility, which results in reproducible SERS signal enhancement. The biological nanoparticles' dwell time in the nano-trap was in the order of minutes, thus allowing SERS spectra to remain in their natural aqueous medium without the need for drying. First, the geometry of the nano-traps was designed considering nanosized bioparticles of 50-150 nm diameter. Further, the systematic investigation of maximum SERS activity was performed using rhodamine 6 G as a probe molecule. The potential of the optimized SERS nano-bowl is shown through distinct spectral features following surface- (polyethylene glycol) and bilayer- (cholesterol) modification of empty liposomes of around 140 nm diameter. Apart from liposomes, the characterization of the highly crosslinked DNA specimens of only 60 nm in diameter was performed. The modification of DNA gel by liposome coating exhibited unique signatures for nitrogenous bases, sugar, and phosphate groups. Further, the unique sensitivity of the proposed SERS substrate displayed distinct spectral signatures for DNA micelles and drug-loaded DNA micelles, carrying valuable information to monitor drug release. In conclusion, the findings of the spectral signatures of a wide range of molecular complexes and chemical morphology of intra-membranes in their natural state highlight the possibilities of using SERS as a sensitive and instantaneous characterization alternative.

1. Introduction

Biological macromolecules such as, lipids and nucleic acids, have drawn attention as biocompatible materials in the development of novel therapeutics and diagnostic devices [1]. The application of nanosized biological relevant particles fabricated from these biomaterials (e.g., liposomes, and DNA) are rapidly expanding against non-communicable (e.g., cancers) and communicable

(e.g., infections) diseases [2–4]. Liposomes, composed of a lipid bilayer, are used to deliver drugs to the target cells and bind with the target directly or by endocytosis. The successful delivery of liposomes to the target cell is known to be influenced by their size. However, current studies demonstrate how surface modifications improve target specificity and the impact of bilayer modifications on guarding the stability of liposomes enroute to their target. To this end, it is essential to characterize the chemical fingerprint of liposomes to ensure that key modifications that influence their functionalities remain intact in vivo [5,6].

The high programmability of DNA has enabled the self-assembly of a variety of DNA nanostructures (e.g., DNA nanogels, DNA micelles) that have controllable size, morphology and which can modulate their surface chemistry via precise display of ligands to target specific cells and tissues [7]. Different approaches are used in designing these nanocarriers (e.g., thermal hybridization, enzyme initiated or chemical functionalization), confirming the accurate assembly of DNA nanogels at the atomic level which can monitor the fabrication process and confirm the presence of targeting ligands [8]. Advanced detection and characterization techniques can also give key insights into the stability of DNA nanostructures and evaluate their drug contents. Considering the cost of preparing DNA-based nanostructures, techniques that require small sample concentration and volume are warranted.

However, the routine characterization, identification, and quantification of bioparticles is still challenging due to the lack of quick, sensitive, and low-cost methods that use low sample concentrations and volumes [1,8]. Among various approaches, nanoparticle tracking analysis (NTA) is quick and useful to find out the size of the nanoparticles by tracking its Brownian motion and measure the zeta potential to determine the surface charge and stability in a liquid suspension [9]. Electron microscopy is useful to provide high-resolution images and insights into the shape, size, morphology, and chemical compositions of nanocarriers [6]. Other methods like enzyme-linked immunosorbent assay (ELISA) detect target specific proteins by immobilizing antibodies. Similarly, flow cytometry uses fluorescent labelled antibodies to quantify bioparticles in a liquid suspension. Although powerful, these methods do not provide the chemical fingerprint of the nanocarriers and are often low throughput, labor-intensive, and not suitable for real-time monitoring of drug delivery and controlled drug release.

Raman spectroscopy is a label-free analytical tool for identification of molecules through chemical fingerprints, excluding extended sample preparation requirements that may damage the target [10]. However, regular Raman scattering is usually very weak, with the small cross-section of nanosized bioparticles additionally providing low intensity compared to the autofluorescence spectroscopy and thus requiring high laser power and long spectrum acquisition time [11,12]. An alternative option is to use surface enhanced Raman spectroscopy (SERS), a technique that offers many folds enhancement in spectrum intensity using plasmonic enhancement of metallic nanoparticles, such as, gold (Au) or silver (Ag) [13–15]. Current literature references describe SERS signal by encapsulating plasmonic nanoparticles within the nanocarriers [16]. This method, albeit good for the characterization, poses challenges such as changes in membrane morphology, alteration of membrane fluidity, it can lead to membrane disruption and may trigger toxicity due to *in vivo* accumulation [17,18]. Alternatively, solid-SERS substrates with defined hot spots provide enhanced Raman spectra without external encapsulation. The drawback in this approach is the high Brownian motion of nanosized bioparticles in suspension, which disrupts the SERS signal intensity and the repeatability [19], putting higher demands in the detection method in terms of speed and sensitivity. Reported strategies to counteract Brownian motion include either drying the bioparticles (causing protein breakdown and conformational changes in the sample) or trapping the carriers in media using conventional laser tweezers [20], microfluidic trapping [21], physical trapping via nano-structured surfaces (e.g., nano-hole) [22] or electrophoretic trapping [23]. Among the methods, trapping using nano-structured surfaces (such as nanocavity, nanopore, etc.) does not add any additional instrumentation and is a straightforward method for high-speed

characterization, providing a higher analyte retention time together with lower detection limit for significant measurements. A few literature references reported the SERS characterization of bioparticles using a curved nanostructure acted as passive trap [23,24]. Besides the passive trapping activity, the curved surface offers high local field enhancement due to the large surface area and light trapping ability [25]. Consequently, the plasmonic nanocavity morphology provides a couple of advantages: a substantial amount of plasmonic enhancement plus integrated barriers that limit the motion of the particles inside the system. Based on the analyte integrity of this approach, it is desirable to develop further topologies that can trap and identify distinct chemical composition and Raman spectral data of diverse nano-carriers. So far, the systematic trapping and analysis of nanosized bioparticles in suspensions with intra-membrane modifications have not been adequately studied in the literature.

Here, we demonstrate a honeycomb-like nano-bowl SERS platform for detection of nanocarriers in aqueous media. The proposed honeycomb inspired nano-bowl SERS substrate, fabricated out of a polydimethylsiloxane (PDMS) film through a self-assembled polystyrene beads (PS) monolayer template, provides a large electric field enhancement and enables localization by passively overcoming the Brownian motion of nanocarriers, thus improving the reproducibility of the SERS signal. The nano-bowl SERS substrate was systematically employed to obtain spectra from liposomes, such as phosphatidylcholine (PC) and phosphatidylethanolamine (PE) in pure form and their membranes modified with cholesterol. DNA nanogels and micelles were further characterized to investigate the efficiency of our proposed nano-bowl substrate. The schematic of the overview of nanocarriers used for the study is presented in Fig. 1.
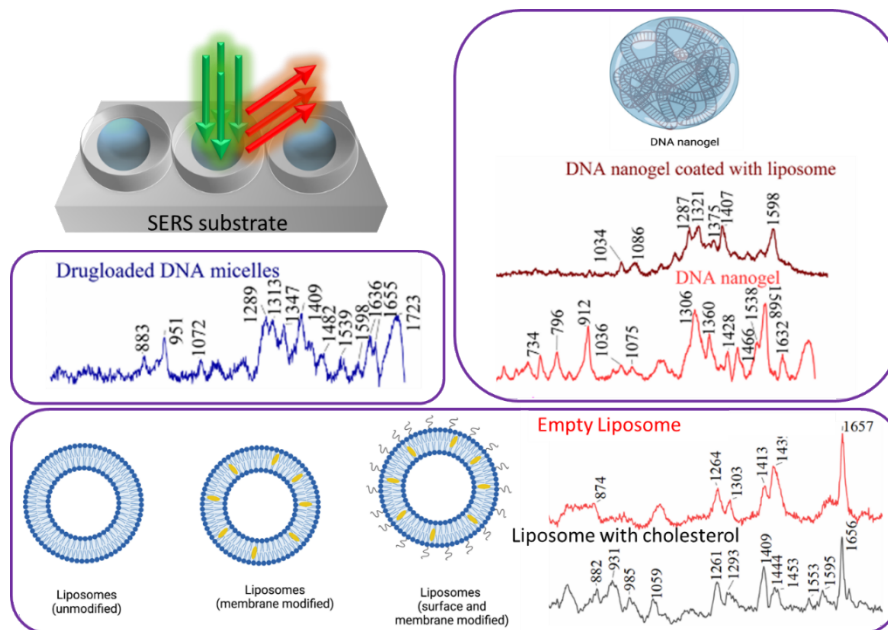

Fig. 1. Overview of analysis of nanosized bioparticles used in this study.

2. Methodology

2.1. Materials

Silicon wafer (Si-Mat), polystyrene beads (190 nm, 500 nm, 1.04 μm diameter, Bangs Laboratories), deionized (DI) water, sodium dodecyl sulfate (SDS) (> 99%, Sigma-Aldrich),

polydimethylsiloxane (SYLGARD184, Dow Chemicals), dichloromethane (>99.8%, Sigma-Aldrich).

2.2. Substrate fabrication details

Nanosphere lithography (NSL) technique was utilized to create nano-bowl structures using three different PS template stamps of 190 nm, 500 nm, and 1 μm in diameter. In the NSL technique, the monolayer of nanospheres, for example, PS beads, is achieved at the air-water interface [26,27]. One method involves spin coating to create a PS bead monolayer. Briefly, spinning a clean wafer or glass plate with a PS bead suspension result in a partial monolayer of beads. The subsequent step includes submerging the beads coated wafer/plate in a hydrophobic solution, causing the beads to ripple in the water and leading the PS beads to arrange into a hexagonally structured self-assembled monolayer (SAM) at the air-water interface. This formed SAM layer can then be transferred to another silicon wafer. Consequently, a large region of silicon wafer is covered by a well-organized 2D array of PS beads.

The nano-bowl PDMS structure was fabricated using three different stamps of PS beads of diameter 190 nm, 500 nm, and 1 μm, respectively. The fabrication steps are schematically depicted in Fig. 2. The fabrication details are provided in the supplementary section 1 in the Supplement 1.
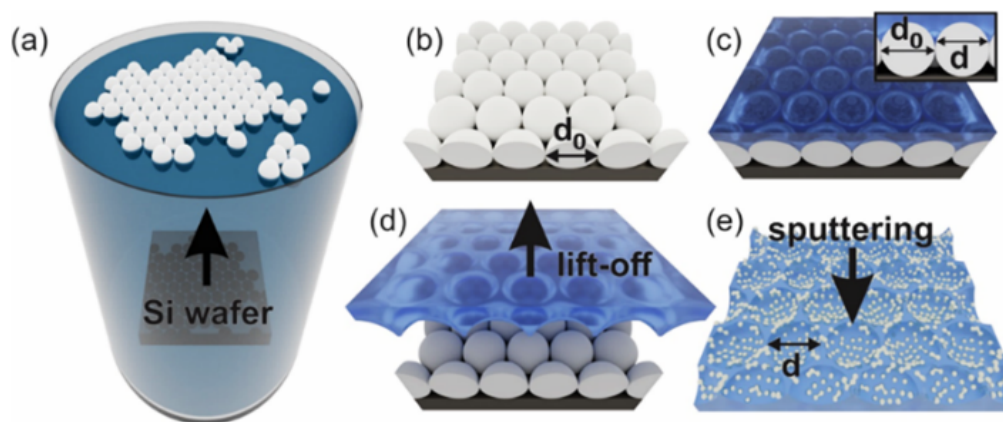

Fig. 2. Schematic representation of the fabrication of the Ag coated PDMS nano-bowl SERS substrate. (a) The monolayer bead template is formed at an air-water interface and (b) adsorbed onto a Si substrate. (c) The monolayer is covered with PDMS, then cured, and (d) peeled off generating a nano-bowl geometry. Note that, PS beads template diameter (d_0) > Nano-bowl diameter. (e) The nano-bowl is further coated with Ag using a sputtering unit.

2.3. Preparation of bioparticles

2.3.1. Synthesis and characterization of liposomes

Liposomal formulations were synthesized via the thin-film hydration method. Pure soy phosphatidylcholine, Liposome S100 (SPC) or SPC containing cholesterol (CHOL) solutions were prepared by dis-solving the lipids in methanol to achieve a percentage molar ratio of 100 (SPC) and 80:20 (SPC/CHOL). For PE containing liposomes, Liposome E PE (EPE), cholesteryl hemisuccinate (CHEMS) and Liposome phosphatidylethanolamine 16:0/16:0 PEG 5000 (PEG 5000) was dissolved in 50:50 solution of chloroform/methanol with or without cholesterol to achieve final percentage molar ratios of 54/41/5 (EPE/CHEMS/PEG 5000) or 44/31/20/5 (EPE/CHEMS/CHOL/PEG 5000) respectively. The solutions were placed under a vacuum at

45 °C for 1 h. Thereafter, the film was rehydrated with phosphate buffered saline (PBS, pH 7.4) to achieve final theoretical concentrations of 10 mg/mL (SPC containing liposomes) or 8.5-8.9 mg/mL (EPE containing liposomes) of the lipids. To promote the formation of homogenous liposomes with high reproducibility, the solutions were then sequentially extruded 6× through each 800 nm, 400 nm, 200 nm, and 100 nm polycarbonate membrane. The liposomes were stored at 4 °C until used. The hydrodynamic diameter and surface charge of the liposomal formulations was determined using dynamic light scattering (DLS) and zeta potential measurements with the NanoZS Zetasizer (Malvern). The size and charge measurement charts are provided in the supplementary table S.T.1 of the Supplement 1.

2.3.2. Synthesis and characterization of DNA nanoparticles

DNA nanogels were prepared as previously described with varying molar ratios of the nanostructures [28,29]. Three DNA nanostructures namely, Y-SAB, Y-SAF and L-SAC were prepared by dissolving the oligonucleotides in 1 × encapsulation buffer (5 mM Tris-HCL, 1 mM EDTA, 10 mM $MgCl_2$, and 10 mM NaCl) and annealed via thermal hybridization for 2.5 h. Equal volumes of the Y-SAF, Y-SAB and L-SAC monomers were then mixed to achieve molar ratios of 4/1/6.5 or 16/4/26 and hybridized at 95 °C. The solutions were then rapidly cooled to 4°C and further incubated for 3.5 h. The hydrodynamic diameter of the nanoparticles was determined with a low-volume quartz cuvette via dynamic light scattering (DLS) with the NanoZS Zetasizer instrument, Malvern.

To prepare the blank DNA micelles, 20 µM of a cholesterol modified DNA sequence (DNA amphiphile) was diluted in 1× Micelle buffer (2.5 mM NaCl, 1.25 mM $MgCl_2$ and 0.05 M sodium acetate, pH 4.5), hybridized at 95 °C and slowly cooled to 4 °C. For the polymyxin B (PMB) loaded DNA micelles, PMB stock solution was prepared in 1× MB and added to 40 µM suspension of the DNA amphiphile to achieve final concentrations of 64 µg/mL PMB as previously reported [30].

The detailed SERS spectral acquisition methodology of bioparticles in suspension state is shown in supplementary figure Fig. S1 of supplementary section 3 in the Supplement 1 file. The oligonucleotide sequences for the DNA nanogel and micelle samples are provided in Table 1(below).

Table 1. Oligonucleotide sequences of DNA-based nanocarriers

Code		Oligonucleotide sequence
Y-SAF	Y_1	GTCTTCGTCCTTATCGGTAGGGTGCTGAGCGGAATC CTGA
	Y_2	GTCTTCGTCCTTTCAGGATTCCGCTCAGTCATGTCATCAC
	Y_3	GTCTTCGTCCTTGTGATGACATGACACCCTACCGAT
Y-SAB	Y_1	ATCGGTAGGGTGCTGAGCGGAATCCTGA
	Y_2	TCAGGATTCCGCTCAGTCATGTCATCAC
	Y_3	GTCTTCGTCCTTGTGATGACATGACACCCTACCGAT
L-SAC	L_1	AAGGACGAAGACGTAGCCTACTATCTTCATTACCAGGTGCAGCC
	L_2	AAGGACGAAGACGGCTGCACCTGGTAATGAAGATAGTAGGCTAC
15bp_chol_ssDNA		5'-ATCGGTAGGGTGTCA/3CholTEG/-3′
15bp_ssDNA		5'-ATCGGTAGGGTGTCA-3'

2.4. SERS spectrum acquisition methodology

All SERS spectra were acquired using a Renishaw In-Via Micro Raman spectrometer with a 50×, 0.75 NA objective, and a 532 nm excitation laser with 0.5 mW power and 5 s integration time. A

10 μL of R6G solution (concentrations ranging from 10^{-6} M – 10^{-15} M) was drop coated on the SERS film and Ag-coated flat film and further dried at the ambient conditions. The films were subsequently washed to remove poorly adsorbed molecules, and spectra were acquired. A rectangular PDMS chamber (1.5 μm thick) was placed on the SERS substrate to acquire the SERS signal from biomolecules in a liquid state. Then, the sample fluid (5 μL in volume) was placed inside the chamber and sealed using a glass coverslip on top of it. The schematic representation of the sample preparation protocol for SERS measurement is shown in Supplement 1. The adopted strategy ensures that the material in the solution does not dry out, preserving its biological value. The standard Raman spectra of SPC, EPE liposomes, DNA nanogels and micelles were collected to compare the enhancement activity. The spectra were acquired considering the same amount (5 μL drop) of sample solution inside a PDMS chamber, placed on a flat Si wafer and/ or flat PDMS film without any Ag coating present on the surface. The solution was further sealed using a glass coverslip from the top. The standard Raman spectra were acquired at a high power of 60 mW and integration time of 60 sec for two acquisitions. For SERS measurements, the incident laser power was varied from 0.5 mWatt-10mWatt considering random spots on each substrate. In this present work, we obtained the SERS signal using DNA nanoparticles in the original buffers that were used to prepare them. Prior to conducting our experiments, we recorded the background signal using the blank buffers as controls. All spectra were collected for two acquisitions, baseline corrected, and background subtracted. Each spectrum shown in the figure is an average of five independent measurements considering the same substrate choosing different locations.

3.   Results and discussions

3.1.   Optimization of SERS substrate

The structural parameters of the nano-bowl SERS chip were optimized inspecting two important parameters: A) the nano-bowl dimensions which should be larger than the bioparticles to be able to entirely trap the particles; and B) the morphology of Ag coating on nano-bowl for enhanced plasmonic activity considering 532 nm excitation wavelength [31].

The smallest size of the bioparticles used in this work was 60 nm for DNA nanogel, and the largest was for liposomes around 150 nm. The first point was addressed considering the PS stamps having diameter of 190 nm, 500 nm, and 1 μm, respectively, being greater than the size of the bioparticles.

The nano-bowl surface topology and uniformity of the nano-bowl array was characterized using FESEM. The morphology of structured PDMS surface cured from polystyrene monolayer beads template of the varying diameters (190 nm, 500 nm, and 1 μm) without Ag coating is shown in Fig. 3(a-c), and with Ag coating in Fig. 3(d-f). The average bowl diameters without any Ag coating were calculated to be 90, 300 and 600 nm, cured from 190, 500 and 1 μm PS beads templates, respectively. As observed from Fig. 3(d-f), with an increase in the amount of Ag coating, the bowl diameter gets filled with Ag.

To optimize Ag coating, the deposition of Ag was varied in thicknesses of 5, 15, and 40 nm. The SERS intensity was monitored using 1 mM R6G as a probe molecule. The SERS spectra of R6G and the corresponding enhancement factor (EF) were calculated and are provided in the supplementary section 3. As seen in supplementary Fig. S2 and supplementary table S.T.2, the 40 nm Ag-coated 600 nm nano-bowl PDMS film (cured from a 1 μm PS template) exhibited the highest enhancement factor, 10^9 higher than a flat PDMS film, surpassing other substrates with diameters of 90 nm (obtained from a 190 nm bead template) and 300 nm (cured from a 500 nm bead template). The likely reason for the maximum SERS activity is attributed to the larger surface area and optimized coating of tightly spaced Ag nanoparticles covering the entire nano-bowl. The FESEM images suggest that the sputtering deposition of Ag led to the formation of nanoparticles instead of a continuous film, and the increasing deposition reduced the nano-bowl curvature, decreasing the effective surface area. It has previously been established
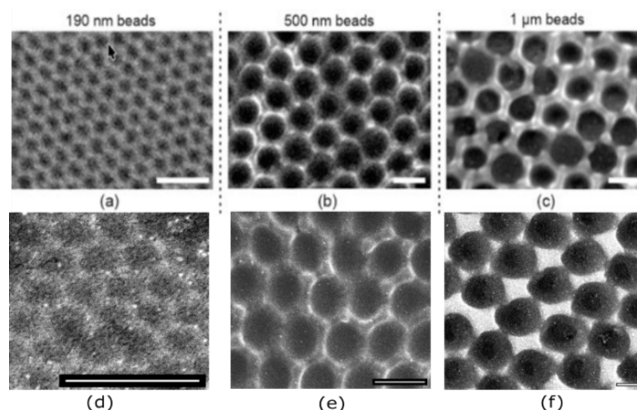
Fig. 3. Field emission scanning electron microscopy (FESEM) image of (a-c) uncoated and (d-f) Ag-coated nano-bowl structured PDMS film cured from a PS template of 190 nm, 500 nm, and 1 μm, respectively. Scale bar: 500 nm. The average bowl diameters without any Ag coating were calculated to be 90, 300 and 600 nm, cured from 190, 500 and 1 μm PS beads templates, respectively.

in literature that the curvature of a surface is beneficial for increased surface area and light-based optical trapping. The SERS enhancement also depends on the shape of the optimized Ag-coated nano-bowl structure to produce an enhanced electric field [29]. In brief, the curved structure, acting as a lens focuses the laser light spot tightly, creating a higher intensity of hotspots compared to the flat surface [30]. The shape anisotropy of the Ag-PDMS film also induces a higher density of hotspots compared to a flat film due to its tightly spaced discontinuous Ag nanoparticles that exhibit strong LSPR for a robust enhancement in the Raman signal. The reproducibility of SERS signal considering eight arbitrary locations on a particular substrate and the limit of detection (10^{-6} to 10^{-15} M) of the optimized SERS substrate were investigated using the R6 G molecule and are shown in supplementary figure Fig. S3 of the Supplement 1 file.

3.2.   Analysis of passive trapping activity

The nano-bowl film has surface topology that can passively trap particles. The principle of particle tracking in the nano-bowls is based on surface topology assisted passive trapping of nanoparticles [23,24]. In brief, the nano-bowl geometry enables the particles to overcome its high Brownian motion. This happens due to the presence of frictional surface barriers that cover each nano-bowl. This method of trapping utilizes the surface to restrict the motion of the nanoparticles on the surface (XY) plane. The motion of the nanoparticles along the Z-direction is influenced by the gradient force of the incident laser along the direction of propagation (calculated depth of focus of laser = 1.02 μm). The laser is incident during the spectrum acquisition. Other nanosized surface topology such as nanoholes, nano-wells, and nanocavity that follow similar principle for the temporary trapping of nanoparticles are previously covered [23,24].

The factors influencing the trapping efficiency and the dwell time of nanoparticles are the shape and dimensions of the nano-bowl, size of the particle and the laser power used for SERS excitation. To evaluate the ability to accommodate particles, we took polystyrene beads (250 nm) and liposomes (150 nm) for a proof-of-concept study. Figure 4(a) shows the SEM image of 250 nm polystyrene nanobeads, demonstrating the localization of individual nanobeads inside nano-bowls.

To evaluate the effectiveness of bioparticle trapping, we tracked the motion of liposomes using a bright-field microscope (60 ×, 1.2 NA water immersion objective lens). The captured
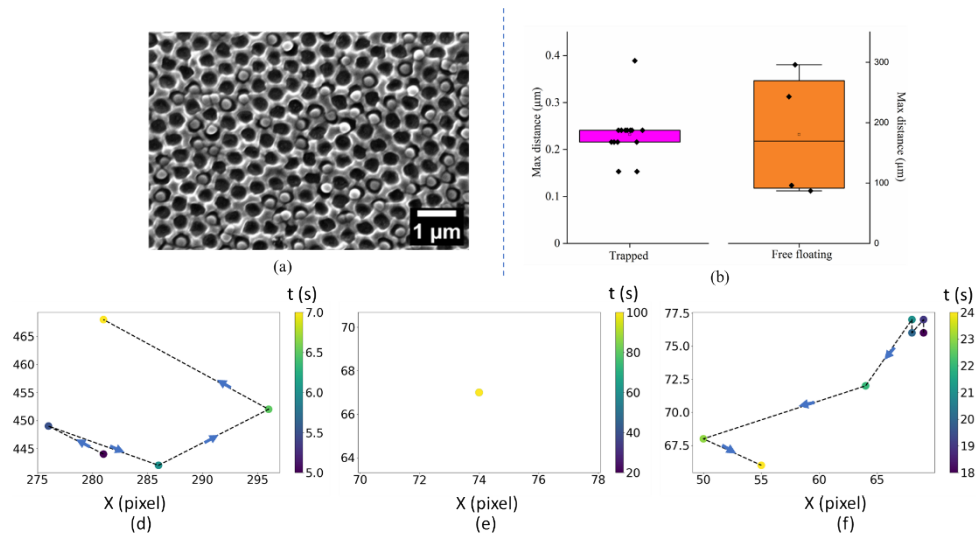
Fig. 4. (a) SEM image of trapped polystyrene beads (250 nm diameter beads) inside the nano-bowl, cured from 1 μm PS template. (b) Shows the maximum displacement of trapped liposome for up to 100 s while the free-floating liposomes were only tracked for up to 4 s due to high Brownian motion. (c) Dynamic track plot of a free-floating liposomes on flat PDMS, (d, e) show trapped and partially trapped liposomes on the nano-bowl shaped PDMS respectively. The plot implies that the trapped liposomes are localized, easy to focus, and while the free and partially trapped liposomes exhibit arbitrary diffusive motion over time. The tracking in (c-e) was only performed in XY plane, the free-floating liposomes had a significant motion along the Z-axis as shown in Supplementary Movie. S.M. 1 and S.M. 2 of Supplement 1.

videos (supplementary movie S.M. 1 and S.M. 2) are made available in Supplement 1., and video snapshots in Supplement 1. The particles' coordinates (X, Y) were extracted using ImageJ software, and the trajectories of non-trapped, entirely trapped, and partially trapped lipids were plotted and shown in Fig. 4(b-e). Motion tracking allowed us to classify the motion of liposomes into three categories:

1. Liposomes free-floating on a flat PDMS film displayed random Brownian motion with rapid in-and-out of focus plane, making them difficult to track even for a few seconds, see Fig. 4(c).

2. Liposomes that were trapped by the honeycomb-like nano-bowl surfaces. Although liposomes tried to escape from the trap, their coordinates remained the same over several minutes making them highly localized, see Fig. 4(d).

3. Liposomes that were assumed to be partially trapped to other liposomes. This occurred when a free-floating liposome attached to another trapped liposome, becoming partially attached to the nano-bowl surface. An example of this is shown in Fig. 4(e) where a liposome continuously moved and eventually escaped the trap after a short interval, for example after 19 seconds as shown in Fig. 4(e).

Thus, the nano-bowl topology is effective for passive trapping of the particles.

3.3. SERS analysis of liposomes

The fabricated SERS substrates were utilized to examine the real-time characterization ability of a diverse set of liposomes, such as SPC, and EPE. We examined two aspects for characterization, suitable for therapeutic application. First, to investigate if nano-bowl SERS substrate can identify two differently composed liposomes and secondly if it can show spectral changes upon membrane modification. Hence, the SERS spectra were examined for two distinct liposomes, and their membrane structure modified with cholesterol, as shown in Fig. 5.
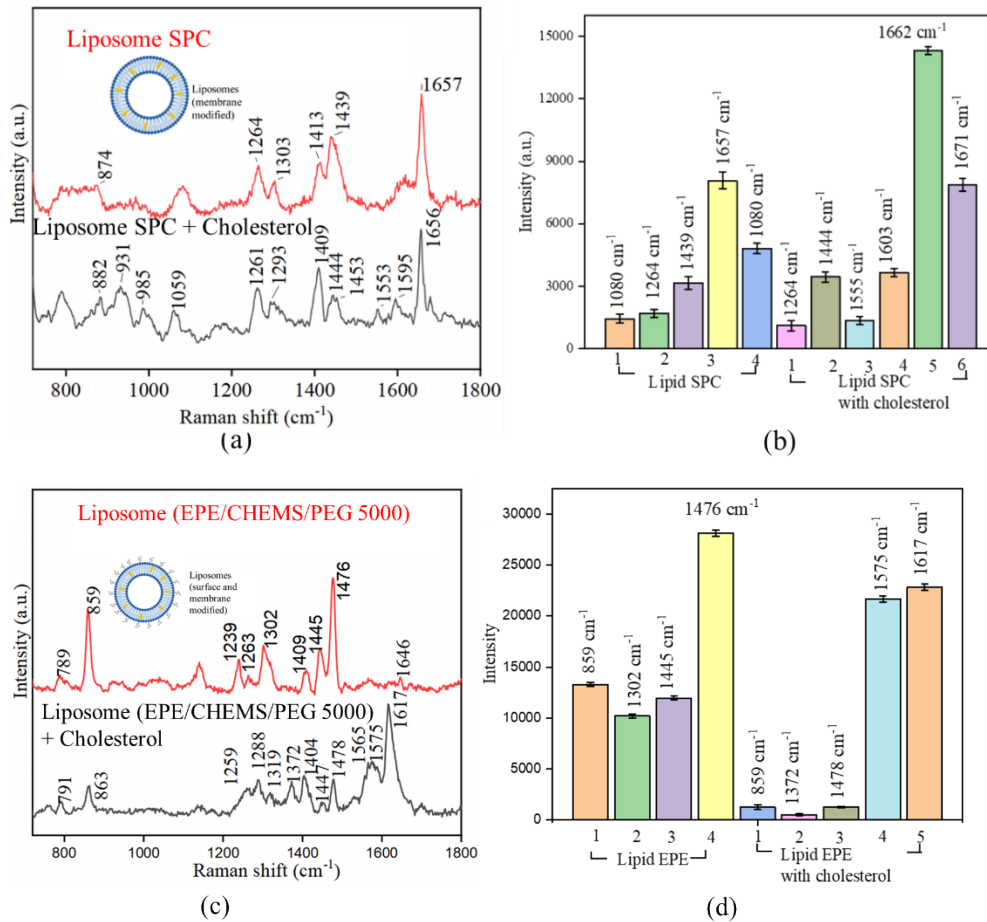

Fig. 5. SERS spectra of liposomes (a) SPC with and without cholesterol, (b) Corresponding intensity plot where error bar denotes the standard deviation in the signal intensity or 10 independent measurements. (c) SERS spectra of EPE liposome with and without cholesterol, (d) displays the corresponding intensity plot for each prominent peak. The specific peaks at 1555, 1671 cm^{-1} are occurred for SPC liposome with cholesterols. For EPE liposome with cholesterol, peaks at 1565, 1575, 1617 cm^{-1} are attributed to cholesterol.

Figure 5(a) shows the Raman spectra of SPC liposome with and without cholesterol, and Fig. 5(b) shows corresponding intensity scale bar. In Fig. 5(a), Liposome SPC exhibits Raman peak at 874, 1264, 1303, 1439, and 1657 cm^{-1} are assigned for lipid bands [32]. The SPC containing cholesterol gives shifted lipid band peak at 882 cm^{-1}. The peak at 1059 cm^{-1} corresponds to stretching of C-C carbonate chains. The peak 1303 cm^{-1} is shifted to 1293 cm^{-1} for SPC with cholesterol. The additional peaks at 1553 and 1595 cm^{-1}, 1737cm^{-1} for ester

linkage of cholesterol. The shift at $1672\,\text{cm}^{-1}$ originates from the $C = C$ stretching vibrations for cholesterol [33].

A close insight into the spectral features shows an enhanced intensity at $1656\,\text{cm}^{-1}$ for SPC with cholesterol (Fig. 5(b)). Additional cholesterol peak intensity mapped at $1555\,\text{cm}^{-1}$ and $1671\,\text{cm}^{-1}$ are also key characteristics of cholesterol presence. An enhanced intensity of $1059\,\text{cm}^{-1}$ is observed for cholesterol added SPC liposome [34].

Figure 5(c) shows the Raman spectra of the liposome EPE (EPE/CHEMS/polyethylene glycol (PEG)) and the EPE liposome containing cholesterol in the membrane, and 5 (d) represents the corresponding intensity plot of Raman shifts. Some additional Raman shift observed at $789\,\text{cm}^{-1}$ arising from the ethanolamine group for phosphatidylethanolamine spectrum [34]. The shift at $859\,\text{cm}^{-1}$ indicates the vibration of choline $N^+(CH_3)_3$ group of phosphatidylcholines. The peak at $1239\,\text{cm}^{-1}$ for EPE/PEG liposome appears twisting of CH_2 bonds for PEG molecule. Peak at $1302\,\text{cm}^{-1}$ for twisting of CH_2 of EPE. A highly intense peak at $1476\,\text{cm}^{-1}$ assigns bending of CH_2 of PE lipid membrane. For EPE liposome with cholesterol, additional Raman peaks at $1372\,\text{cm}^{-1}$, and an intense peak at $1617\,\text{cm}^{-1}$ were observed. The additional peak at $1372\,\text{cm}^{-1}$ occurs due to CH_2 twisting mode of cholesterol oleate. The Raman peaks at 1565, 1575, and $1617\,\text{cm}^{-1}$ are specific Raman peaks of cholesterol. The standard Raman spectra of both liposome samples were acquired, and the SERS spectrum reproducibility was investigated, shown in supplementary sections 4 with supplementary figure Fig. S5 and Fig. S6, respectively.

The surface modification of EPE liposome using PEG/CHEMS was found to exhibit improved SERS intensity (overall 2-fold enhancement in Raman peaks), as shown in Fig. 5(d). In the supporting information file, a comparison of regular Raman and SERS intensity was provided in supplementary figure Fig. S5 to further support this fact. The improved SERS performance can be attributed to the surface modification (hydrophilicity) achieved using CHEMS/PEG. PEG is commonly used for stabilizing Ag nanoparticles, and this improved surface adhesion can affect SERS measurements [34]. Additionally, PEG-functionalized liposomes exhibit better hydrophilicity and stability. Thus, the improved hydrophilicity could improve adsorption of Ag nanoparticles with the liposomes generating higher signal intensity. However, the thickness of the PEG layer affects the SERS signal, and it could potentially obscure the bilayer Raman signal. To better describe the impact of the PEG thickness on this, there is a need to monitor the impact of increasing PEG molar ratios and alteration of PEG on the SERS signals in future studies. In summary, the evolved measurement technique allows for the sensing of both surface and bi-layer modifications simultaneously, providing a useful tool for real-time characterization.

3.4.   SERS analysis of DNA

Complex DNA models, such as DNA nanogel and micelles, were utilized and characterized to check the feasibility of the PDMS nano-bowl as the SERS substrate. The formation of the crosslinked DNA nanogels was previously confirmed, and their sizes were characterized with DLS. As shown in Supplement 1, the DNA nanogels revealed sizes of 62 nm, which agrees with previous reports providing a model for SERS analysis [10,35]. We focused on addressing some crucial questions to investigate the molecular signature of the complex sample, such as, DNA nanogel and micelles: A) Instant characterization of self-assembled DNA nanoparticle via monitoring spectra changes of the monomers, B) Detection of intra-membrane changes upon modification (such as, liposome coated nanogel, drug loaded micelles).

To address the first point, we acquired SERS spectra of DNA nanogel, DNA micelles and their building blocks. In brief, the DNA nanogels are prepared using 3 nanostructures which bear a Y-shape (composed of three single strand DNA (ssDNA) that anneal into a Y-shape) and an L-shape (the linker is composed of 2 ssDNA sequences that anneal into a double stranded helix resembling an L-shape). The nanostructures therefore bear variations in shape (structural) and composition (two strands of DNA versus three strands of DNA). In Fig. 6(a), the SERS

spectra of nanostructured monomers i.e., the Y-scaffold, L- linker and Y-blocking, are displayed. The peak at $791 \, \text{cm}^{-1}$ present in linker undergoes a blueshift compared to the scaffold and the blocking samples. For the L-linker, the Raman bands exhibit a notable decrease in strength, and a reduced number of enhanced modes. The observed alterations may be attributed to the structural modification in the L-linker compared to Y scaffold and Y blocking. Many characteristic Raman bands are detected in the crosslinked nanogel sample which could be linked with scaffold, linker, and blocking units. For instance, the intense peak at $732 \, \text{cm}^{-1}$ for the Y-scaffold and Y-blocking, assigned for the ring breathing mode of adenine (A), is shifted to $734 \, \text{cm}^{-1}$ in the DNA nanogel. The peak at $795 \, \text{cm}^{-1}$, assigned for poly C and poly T ring breathing mode, is present in all the building blocks and the crosslinked nanogel. The less intense peak at $962 \, \text{cm}^{-1}$ for deoxyribose, 1007, $1165 \, \text{cm}^{-1}$ for dT, dA, and $1245 \, \text{cm}^{-1}$ for vibration of cytosine is detected in the scaffold sample. The intense peak at $1324 \, \text{cm}^{-1}$ for adenine for Y scaffold is shifted at $1330 \, \text{cm}^{-1}$ in the blocking sample. The peak at $1391 \, \text{cm}^{-1}$ is a characteristic peak and is present only in the scaffold. The shift at $1426 \, \text{cm}^{-1}$, indicating C_2H_2 bonding (B, Z DNA) in blocking, is shifted at $1428 \, \text{cm}^{-1}$ in the nanogel sample. The peak at $1463 \, \text{cm}^{-1}$, indicating ATC in scaffold samples, is shifted at $1466 \, \text{cm}^{-1}$ in the formed nanogel. The intense peak at $1488 \, \text{cm}^{-1}$ corresponds to the cytosine (C) peak in Y-blocking. The less intense shift at $1007 \, \text{cm}^{-1}$ for PO_2^- stretching of backbone, and $1075 \, \text{cm}^{-1}$ for OPO symmetric stretching in the nanogel sample is associated with scaffold. The Raman signature of the scaffold at $1463 \, \text{cm}^{-1}$ for A, T, and C is shifted at $1466 \, \text{cm}^{-1}$. The peak at $1515 \, \text{cm}^{-1}$ corresponding to C occurs at $1538 \, \text{cm}^{-1}$ in the nanogel sample. The pyrimidine stretching of adenine at $1529 \, \text{cm}^{-1}$ for linker is shifted to $1538 \, \text{cm}^{-1}$ after nanogel formation. The shift at $1545 \, \text{cm}^{-1}$, $1575 \, \text{cm}^{-1}$, and $1596 \, \text{cm}^{-1}$ occurs for the adenine band [35]. The crosslinked nanogel exhibited a larger peak intensity at $861 \, \text{cm}^{-1}$ for asymmetric stretching indicating the increase in deoxyribose after crosslinking. The peak at $1463 \, \text{cm}^{-1}$ in scaffold has shifted to $1473 \, \text{cm}^{-1}$ after crosslinking. The weak peak at $1521 \, \text{cm}^{-1}$ in linker is intense and present at $1519 \, \text{cm}^{-1}$ in the nanogel. The shift at $1568 \, \text{cm}^{-1}$ is ascribed to purine mode. A broad carbonyl stretching band is present at $1632 \, \text{cm}^{-1}$ in the nanogel. The distinct peak at 1726cm^{-1} is assigned for the $(C=O)$ bond of dG. The nanostructures have at least one short ssDNA strand at their ends (sticky ends) to initiate nanogel formation. Comparing the two Y-shaped monomers, two of the sticky ends on the Y-scaffold are truncated to form the Y-blocking unit and this variation in the number of sticky ends translated into significant variation in the number of Raman peaks. This is likely the reason we observed a gradual increase in the number of intense peaks for the Y-scaffold compared to the Y-blocking and L-linker. Additionally, the weak peaks at 962, 1007, 1102 and $1165 \, \text{cm}^{-1}$ occur due to the deoxyribose-linked phosphodiester network in the scaffold and is present in the crosslinked nanogel [35,36]. Hence, the SERS spectrum shows the structure related Raman bands, indicating the possibility of SERS based label-free detection of DNA nanogel using the developed methodology.

A modification of nanogel by liposome coating was performed to detect the chemical changes in the spectral changes of nanogel upon coating (Fig. 6(a)), and corresponding intensity plot is shown in 6(b). As evident from Fig. 6(a), the strong peak at 734, $796 \, \text{cm}^{-1}$ for adenine is diminished for the liposome-coated DNA nanogel sample. The ratio of the signal intensity at the Raman shift for the $645 \, \text{cm}^{-1}$ and $796 \, \text{cm}^{-1}$ peaks is calculated to be greater than 1 when considering the nanogel compared to the coated nanogel samples. Additionally, the peak intensity of phospholipid for liposome-coated DNA was much larger (~9 times) than that of the nanogel samples. The peaks at 1287 and $1321 \, \text{cm}^{-1}$ indicate CH_2 deformation of lipids. The peak at $1360 \, \text{cm}^{-1}$ is shifted to $1375 \, \text{cm}^{-1}$ in the coated nanogel. The intense peak at $1598 \, \text{cm}^{-1}$ is attributed to the adenine band of DNA. Thus, the modification of liposomes on DNA nanogel exhibited characteristic peaks of phospholipids and DNA bases.

Next, DNA micelles were characterized to enquire about spectra changes in the DNA amphiphile following self-assembly of the micelles. Micelle formation is characterized by
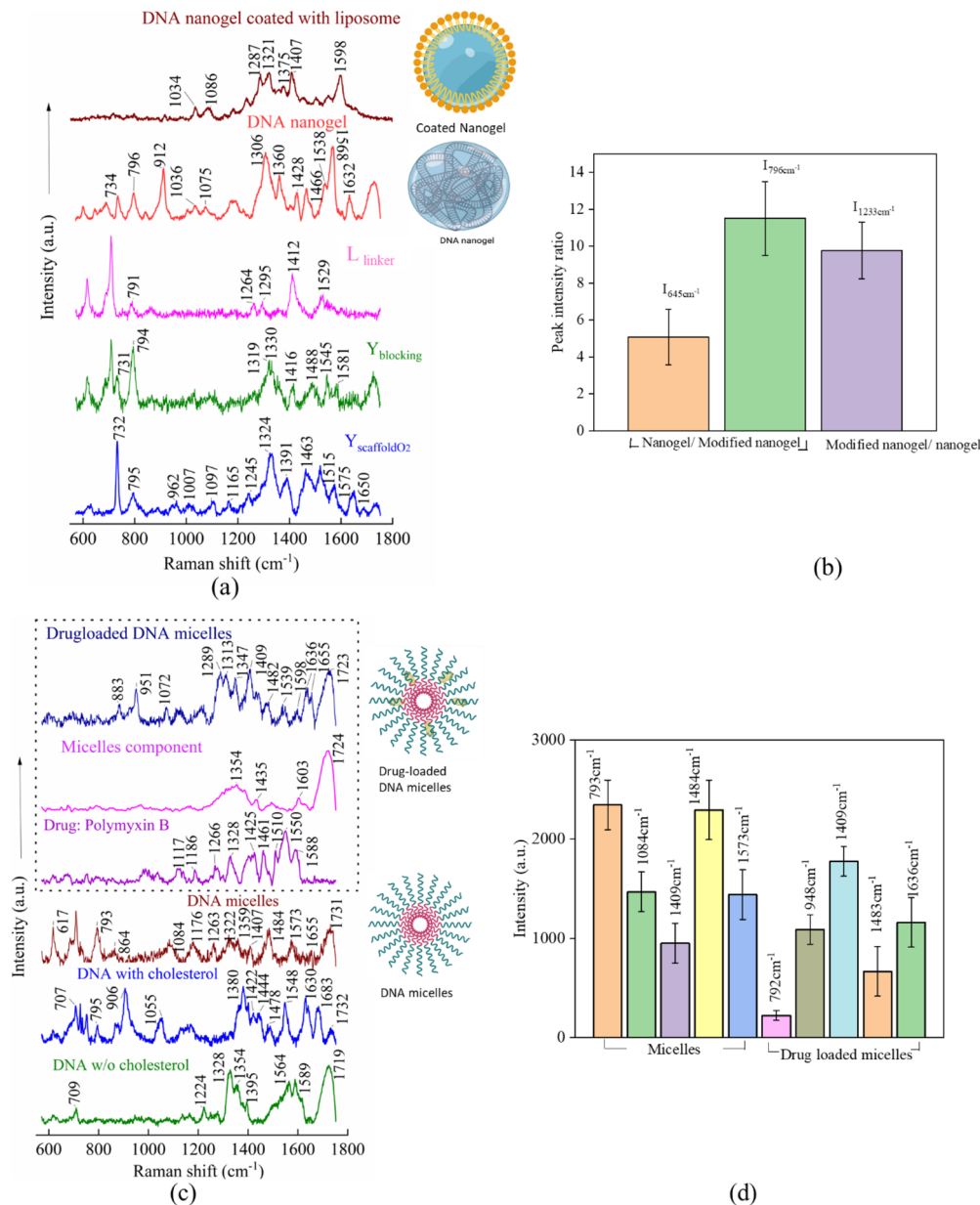
Fig. 6. Comparison of complex DNA specimens: SERS spectra of (a) components of DNA nanogels, nanogel, and modified nanogel membrane with liposome. Equal volumes of the Y-SAF, Y-SAB and L-SAC monomers were then mixed to achieve molar ratios of 4/1/6.5 or 16/4/26 and hybridized at 95 °C for nanogel formation. (b) SERS intensity ratio of Raman features of nanogel and coated nanogel for quantifying signal fluctuations where coating subsequently diminish peaks of DNA ($645\,\text{cm}^{-1}$ and $796\,\text{cm}^{-1}$) and enhance characteristics peaks of liposome ($1233\,\text{cm}^{-1}$). (c) Characterization of DNA micelles: comparison of micelles with pure DNA, and DNA with cholesterol. Comparison of Drug loaded DNA micelles with individual components of the solution for making drug loaded micelles (highlighted in rectangular box). (d) Corresponding intensity plot where error bar denotes the standard deviation in the signal intensity for 10 independent measurements. The spectrum changes are useful to evaluate controlled drug release.

cholesterol aggregation in the core of the particle while the DNA sequence comprises the corona. So, investigating micelles would exhibit molecular signatures of the combination of DNA and cholesterol. Figure 6(c) shows the SERS spectra of DNA, DNA with cholesterol and the self-assembled DNA micelles. The characteristic bands of DNA exhibited sharp features at $617\,cm^{-1}$ for ring deformation, and $726\,cm^{-1}$ for in-plane ring breathing of A. The Raman shift at $798\,cm^{-1}$ for in-plane ring breathing, and $902\,cm^{-1}$ for asymmetric C-H wagging of C. The shift at $682\,cm^{-1}$ and $874\,cm^{-1}$ are ascribed for ring deformation, and N-H wagging modes of G. The peaks at 709, 1224, and $1328\,cm^{-1}$ were assigned for G ring breathing, $1354\,cm^{-1}$, $1564\,cm^{-1}$ and $1589\,cm^{-1}$ for A, $1395\,cm^{-1}$ for C band. The incorporation of cholesterol into the DNA sample causes peak shifts and the addition of new characteristic peaks of cholesterol, such as 1548, 1630, and $1683\,cm^{-1}$. The phosphate backbone Raman intensity at 906 and $1055\,cm^{-1}$ is also increased in cholesterol-modified DNA.

The Raman peak of DNA micelles indicates inclusive features of cholesterol and DNA bases. A new peak at $1484\,cm^{-1}$ is the signature peak of ATC in micelles. The Raman peak at $1380\,cm^{-1}$ is shifted to $1407\,cm^{-1}$, the peak at $1478\,cm^{-1}$ appears at $1484\,cm^{-1}$, and $1548\,cm^{-1}$ to $1573\,cm^{-1}$ for the micelle sample.

To evaluate the composition of drug-loaded (polymyxin B-PMB) micelles, a close comparison of the final PMB loaded micelles and its individual monomers prior to mixing was performed. As evident in Fig. 6(c) the polymyxin B drug exhibited sharp molecular features at 1266, 1328, 1510, and $1550\,cm^{-1}$, which is shifted at 1289, 1347, 1539, and $1598\,cm^{-1}$ in the drug-loaded micelles. The peak of unperturbed DNA micelles at 1347, 1484, 1655, and $1731cm^{-1}$ appeared at 1359, 1482, 1655, and $1723cm^{-1}$, respectively. Figure 6(d) shows the intensity scale to facilitate a better comparison of peak intensities of empty micelles and drug load micelles. The presence of polymyxin B into micelles causes blue shift in peak position that could potentially be due to the formation of new complexes. Thus, the molecular information of PMB micelles revealed inclusive peaks of micelles and loaded drugs. The SERS spectrum reproducibility was performed for six different positions of a SERS substrate (Supplement 1.) considering different laser powers, independent locations on the substrate, and substrates from different batches. The spectral intensity variation was calculated to be less than 10%.

4. Conclusion

We developed and validated a methodology to fabricate Ag-coated nano-bowl to trap and characterize nanosized liposomes, DNA-gel, and micelles. The trapping was possible due to the surface topography of the novel nano-bowl pattern. The SERS signals of liposomes with and without any modification in the membrane were extracted using the proposed nano-bowl design. The modification of the liposome samples with PEG exhibited additional peaks in comparison to the liposomes without PEG. The membranes of the SPC and EPE liposomes exhibited different vibrational peaks, indicating the possibility of using nano-bowl SERS substrate to determine different membrane composition of liposomes (160 nm) in wet condition. Interestingly, incorporation of cholesterol in liposome membrane exhibited additional Raman features for distinction. Understanding the membrane composition and molecular changes in liposomes allows the customization of drug carriers with improved characteristics. Hence, the methodology could be beneficial in designing more efficient and targeted drug delivery vehicles, improving drug release profiles, and minimizing undesired side effects.

Further, the SERS methodology enabled identification and characterization of DNA nanogel, and DNA micelles that could be useful for personalized medicine. The coating of DNA nanogel with liposome included features of phospholipid. The drug loaded micelles exhibited inclusive Raman peaks of micelles and drugs. Hence, the proposed substrate is capable of sensing molecular changes at the surface, which could be helpful for the instant identification of distinct membrane compositions in liposomes or specific features in DNA nanogels. It enables the

development of therapies that precisely target underlying molecular conditions. Therefore, the investigation aimed to develop a proof-of-concept method to provide valuable details about bioparticles without additional chemical reactions, or multiple characterization steps. In future, the presented fabrication method could be extended to the patterning of piezoelectric films such as PVDF for electrochemical SERS, where applied current can tune hotspot activity. In addition to a single layer of Ag, the combination of Ag and Au nanoparticles [37] or dielectric gap-layer [27] in nano-bowls can provide higher sensitivity. In addition to the liposomes, other nanosized analytes such as extracellular vesicles, considered a disease bio-marker could also be explored. Similarly, micrometer sized pathogenic bacteria would be relevant towards antimicrobial resistance studies [12].

Disclosures. The authors declare no conflicts of interest.

Data availability. Data underlying the results presented in this paper are not publicly available at this time but may be obtained from the authors upon reasonable request.

Supplemental document. See Supplement 1 for supporting content.

References

1. L. H. Goetz and N. J. Schork, "Personalized medicine: Motivation, challenges, and progress," Fertil. Steril. **109**(6), 952–963 (2018).
2. P. Chen, L. Wang, X. Fan, *et al.*, "Targeted delivery of extracellular vesicles in heart injury," Theranostics **11**(5), 2263–2277 (2021).
3. A. Ziegler, A. Koch, K. Krockenberger, *et al.*, "Personalized medicine using DNA biomarkers: A Review," Hum. Genet. **131**(10), 1627–1638 (2012).
4. P. Basnet and N. Skalko-Basnet, "Curcumin: An anti-inflammatory molecule from a curry spice on the path to cancer treatment," Molecules **16**(6), 4567–4598 (2011).
5. K. S. Ahmed, S. A. Hussein, A. H. Ali, *et al.*, "Liposome: Composition, characterisation, preparation, and recent innovation in clinical applications," Journal of Drug Targeting **27**(7), 742–761 (2019).
6. C. Chen, S. Zhu, T. Huang, *et al.*, "Analytical techniques for single-liposome characterization," Anal. Methods **5**(9), 2150 (2013).
7. B. Shao and Z. Xiao, "Recent achievements in exosomal biomarkers detection by nanomaterials-based optical biosensors - A Review," Anal. Chim. Acta **1114**, 74–84 (2020).
8. A. A. Attama, P. O. Nnamani, O. B. Onokala, *et al.*, "Nanogels as Target Drug Delivery Systems in cancer therapy: A review of the last decade," Front. Pharmacol. **13**, 1 (2022).
9. M. Wright and Matthew Wright, "Nanoparticle Tracking Analysis," Encyclopedia of Nanotechnology, Encyclopedia of Nanotechnology **2**, 2555–2565 (2016).
10. S. Das, K. Saxena, L. P. Goswami, *et al.*, "Mesoporous AG–Tio2 based nanocage like structure as sensitive and recyclable low-cost SERS substrate for biosensing applications," Opt. Mater. **125**, 111994 (2022).
11. J. Z. Zhang, D. A. Wheeler, A. M. Schwartzberg, *et al.*, "Basics and practice of surface enhanced Raman scattering (SERS) and Tip Enhanced Raman scattering (TERS)," Biomed. Spectrosc. Imaging **3**(2), 121–159 (2014).
12. S. Das, K. Saxena, J.-C. Tinguely, *et al.*, "SERS nanowire chip and machine learning-enabled classification of wild-type and antibiotic-resistant bacteria at species and strain levels," ACS Appl. Mater. Interfaces **15**(20), 24047–24058 (2023).
13. S. Das, K. Saxena, and D. S. Mehta, "A highly sensitive SERS substrate based on a mesoporous AG–tio2 thin film for the detection of Dye Molecules," Mater. Adv. **3**(13), 5337–5343 (2022).
14. S. Das, L. P. Goswami, J. Gayathri, *et al.*, "Fabrication of low cost highly structured silver capped aluminium nanorods as SERS substrate for the detection of biological pathogens," Nanotechnology **32**(49), 495301 (2021).
15. K. Masui, Y. Nawa, S. Tokumitsu, *et al.*, "Detection of glutamate encapsulated in liposomes by optical trapping Raman spectroscopy," ACS Omega **7**(11), 9701–9709 (2022).
16. Y. Ren, Q. Chen, M. He, *et al.*, "Plasmonic Optical Tweezers for particle manipulation: Principles, methods, and applications," ACS Nano **15**(4), 6105–6128 (2021).

17. M. Faried, K. Suga, Y. Okamoto, *et al.*, "Membrane surface-enhanced Raman spectroscopy for cholesterol-modified lipid systems: Effect of gold nanoparticle size," ACS Omega **4**(9), 13687–13695 (2019).

18. W. Yao and C. I. Kim, "A lipid membrane morphology subjected to intra-membrane viscosity and membrane thickness dilation," Continuum Mech. Thermodyn. **35**(2), 645–667 (2023).

19. C. Zong, M. Xu, L.-J. Xu, *et al.*, "Surface-enhanced Raman spectroscopy for bioanalysis: Reliability and challenges," Chem. Rev. **118**(10), 4946–4980 (2018).

20. J. Wang, Y. C. Kao, Q. Zhou, *et al.*, "An integrated microfluidic-sers platform enables sensitive phenotyping of serum extracellular vesicles in early stage melanomas," Adv. Funct. Mater. **32**(3), 2010296 (2022).

21. L. Kaufman, T. Cooper, G. Q. Wallace, *et al.*, "Trapping and SERS identification of extracellular vesicles using nanohole arrays," Proc. SPIE, **10894**, 108940B (2019).

22. C. T. Ertsgaard, N. J. Wittenberg, D. J. Klemme, *et al.*, "Integrated nanogap platform for sub-volt dielectrophoretic trapping and real-time Raman imaging of biological nanoparticles," Nano Lett. **18**(9), 5946–5953 (2018).

23. C. Lee, R. P. Carney, S. Hazari, *et al.*, "3D plasmonic nanobowl platform for the study of exosomes in solution," Nanoscale **7**(20), 9290–9297 (2015).

24. X. Yan, H. Shi, P. Jia, *et al.*, "Tunable plasmonic tweezers based on nanocavity structure for multi-site trapping," Optica Open 107688, 2023.

25. C. S. Liu and V. K. Tripathi, "Optical gain in surface plasmon nanocavity oscillators," J. Nanophotonics **10**(1), 016015 (2016).

26. Z. Yi, G. Niu, J. Luo, *et al.*, "Ordered array of AG semishells on different diameter monolayer polystyrene colloidal crystals: An ultrasensitive and reproducible SERS substrate," Sci. Rep. **6**(1), 32314 (2016).

27. S. Das, J.-C. Tinguely, V. Kundu, *et al.*, "Sculptured silicon nanopillars bridging face to face nanogaps with metal-insulator-metal coating for surface enhanced Raman spectroscopy," Surf. Interfaces **44**, 103836 (2024).

28. S. Obuobi, K. Julin, E. G. A. Fredheim, *et al.*, "Liposomal delivery of antibiotic loaded nucleic acid nanogels with enhanced drug loading and synergistic anti-inflammatory activity against S. Aureus intracellular infections," J. Controlled Release **324**, 620–632 (2020).

29. S. Obuobi, V. Mayandi, N. A. Nor, *et al.*, "Nucleic acid peptide nanogels for the treatment of bacterial keratitis," Nanoscale **12**(33), 17411–17425 (2020).

30. A. Sousa, V. Borøy, S Baeverud, *et al.*, "Polymyxin B Stabilized DNA Micelles for Sustained Antibacterial and Antibiofilm Activity against P. Aeruginosa," J. Mater. Chem. B **11**(33), 7972–7985 (2023).

31. W. Liu, Y. Li, Z. Li, *et al.*, "3D flexible compositing resonant cavity system for high-performance SERS sensing," Opt. Express **31**(4), 6925 (2023).

32. V. Živanović, Z. Kochovski, C. Arenz, *et al.*, "SERS and Cryo-em directly reveal different liposome structures during interaction with gold nanoparticles," J. Phys. Chem. Lett. **9**(23), 6767–6772 (2018).

33. K. Czamara, K. Majzner, M. Z. Pacia, *et al.*, "Raman spectroscopy of lipids: A Review," J. Raman Spectrosc. **46**(1), 4–20 (2015).

34. K. Nakamura, K. Yamashita, Y. Itoh, *et al.*, "Comparative studies of polyethylene glycol-modified liposomes prepared using different PEG-modification methods," Biochim. Biophys. Acta, Biomembr. **1818**(11), 2801–2807 (2012).

35. P. Šimáková, J. Gautier, M. Procházka, *et al.*, "Polyethylene-glycol-stabilized AG nanoparticles for surface-enhanced Raman scattering spectroscopy: Ag surface accessibility studied using metalation of 12free-base porphyrins," J. Phys. Chem. C **118**(14), 7690–7697 (2014).

36. S. J. Friedman and A. C Terentis, "Analysis of G-Quadruplex Conformations Using Raman and Polarized Raman Spectroscopy," J. Raman Spectrosc. **47**(3), 259–268 (2016).

37. Fu-Hsiang Ko, Ming-Rou Tai, Ken Liu, *et al.*, "Au–ag core–shell nanoparticles with controllable shell thicknesses for the detection of adenosine by surface enhanced Raman scattering," Sens. Actuators, B **211**, 283–289 (2015).